Electronic Supplementary Information

A cobalt(II) bis(salicylate)-based ionic liquid that shows thermoresponsive and selective water coordination

Yuki Kohno,[a] Matthew G. Cowan,[a] Miyuki Masuda,[b] Indrani Bhowmick,[c] Matthew P. Shores,[c] Douglas L. Gin*,[a,d] and Richard D. Noble*,[a]

[a]Dept. of Chemical & Biological Engineering, and [d]Dept. of Chemistry & Biochemistry, University of Colorado, Boulder, CO 80309, USA. *E-mail: gin@spot.colorado.edu; nobler@colorado.edu; Fax: +1-303-492-8595; Tel: +1-303-735-1107*

[b]Dept. of Biotechnology and Life Science, Tokyo University of Agriculture and Technology, 2-24-16, Naka-cho, Koganei, Tokyo 180-8588, Japan.

[c]Dept. of Chemistry, Colorado State University, Fort Collins, CO 80523, USA.

1. Materials and Instrumentation

Tetra-*n*-butylphosphonium hydroxide ($[P_{4444}]OH$), cobalt(II) chloride hexahydrate ($Co^{II}(H_2O)_6Cl_2$), and all solvents were purchased from Sigma-Aldrich. Salicylic acid (H_2Sal) and lithium salicylate (LiHSal) were purchased from Tokyo Chemical Industry Co. All of the chemicals and other solvents were used as received for synthesis. For equilibrium binding studies, all solvents were dried over anhydrous magnesium sulphate and filtered before use. Elemental analysis of the prepared MCIL was performed with a Vario EL III (Elementar) instrument at the Tokyo University of Agriculture and Technology. Differential scanning calorimetry (DSC) was performed with a DSC-6220 instrument (Seiko Instruments Inc.) at a heating rate of 5 °C min^{-1}. Thermogravimetric analysis (TGA) was performed with an EXSTAR TG/DTA 7200 system (Seiko Instruments Inc.) at a heating rate of 10 °C min^{-1}. UV-visible spectroscopy was performed using a UV-2450 instrument (SHIMADZU). Attenuated total reflectance Fourier-transform infrared (ATR-FTIR) spectroscopy was performed with a Nicolet 6700 system (Thermo Scientific). Polarised light microscopy (PLM) studies were performed using a Leica DMRXP polarising light microscope equipped with an Optronics or a QImaging Micropublisher 3.3 RTV digital camera assembly. Regular microscopy studies were performed using the same PLM equipment by taking off the polarisers.

2. Synthesis of $[P_{4444}]_2[Co^{II}(Sal)_2]$

The synthetic procedure used to obtain the MCIL $[P_{4444}]_2[Co^{II}(Sal)_2]$ is shown in Scheme S1. First, tetra-*n*-butylphosphonium salicylate ($[P_{4444}][HSal]$) was prepared according to a previous report.[1] Subsequently, individual aqueous solutions of $[P_{4444}][HSal]$ and LiHSal were prepared and then added dropwise to an aqueous solution of $Co^{II}(H_2O)_6Cl_2$ at a 0.5/1.0/1.0 molar ratio of

$Co^{II}(H_2O)_6Cl_2$/$[P_{4444}][HSal]$/LiHSal. A deep purple liquid immediately separated from water and was extracted using CH_2Cl_2. The CH_2Cl_2 layer was then repeatedly washed with water until no halides were detected by reaction with silver nitrate, and subsequently evaporated to dryness. Next, the obtained liquid was dissolved in methanol and stirred for 24h, during which a small amount of precipitate was observed to form. After filtration of the precipitate, the resulting methanol solution was evaporated and dried in vacuo at 60 °C for at least 24 h. The resulting dark blue liquid was characterised as $[P_{4444}]_2[Co^{II}(Sal)_2]$ (79% yield) by elemental analysis; magnetic moment measurement with ^{1}H-NMR; ATR-FTIR; UV-visible spectroscopy; and magnetic susceptibility studies as described in more detail in sections 3 to 5 below (also see Figs. S1 to S11 and Table S1). Because the product was paramagnetic, it was not possible to perform traditional structural characterisation by ^{1}H and ^{13}C NMR spectroscopy due to severe NMR peak broadening.

3. Elemental Analysis

Elemental analysis of the obtained MCIL was consistent with a chemical composition of $[P_{4444}]_2[Co^{II}(Sal)_2]$ as shown in Scheme S1. The precipitate that formed during the synthetic process was identified as $Co^{II}(OH)(HSal)(H_2O)$, which was previously reported as metal-organic Co(II) hydroxide nanorods.[2]

$[P_{4444}]_2[Co^{II}(Sal)_2]$:
Found: C, 65.33; H, 9.45; N, 0. Calc. for $C_{46}H_{80}CoO_6P_2$: C, 65.00; H, 9.49; N, 0%.

$Co^{II}(OH)(HSal)(H_2O)$:
Found: C, 36.94; H, 3.21; N, 0. Calc. for $C_7H_8CoO_5$: C, 36.39; H, 3.49; N, 0%

4. Calculation of magnetic moment for $[P_{4444}]_2[Co^{II}(Sal)_2]$ in solution by the Evans method

The magnetic moment of $[P_{4444}]_2[Co^{II}(Sal)_2]$ in solution was calculated by the Evans NMR method:[3,4] A 9:1 (v/v) mixture of CD_2Cl_2 and CH_2Cl_2 was dried over anhydrous $MgSO_4$ and immediately used to prepare a 15 mM solution of $[P_{4444}]_2[Co^{II}(Sal)_2]$. The solution of $[P_{4444}]_2[Co^{II}(Sal)_2]$ was then placed within the outer segment of a co-axial NMR tube. The inner segment of the co-axial NMR tube was filled with the original solvent mixture. The ^{1}H-NMR spectrum was collected using a Varian INOVA 400 MHz NMR spectrometer at 295 K and then at increasing temperatures from 178 K to 298 K at 20 K intervals. The frequency difference between the signals corresponding to CH_2Cl_2 in the neat and $[P_{4444}]_2[Co^{II}(Sal)_2]$ solutions was determined and used in the following equation to determine x_g:

$$x_g = -3\Delta f / 4\pi f \mathrm{m} + x_0$$

where: x_g = the mass susceptibility of the material (g^{-1}); Δf = the frequency difference between proton signals from the neat and doped solvent (Hz); f = the frequency of the spectrometer (Hz); m = the concentration of $[P_{4444}]_2[Co^{II}(Sal)_2]$ in the sample (g mL^{-1}). (Note: this value varies with

temperature due to changes in solvent density);[5] and x_0 = the mass magnetic susceptibility of the solvent.

The molar susceptibility x_m is then calculated using the following equation:

$$x_m = x_g \cdot \mathrm{M_w} + x_{\mathrm{Di}}$$

where: x_m = the molar susceptibility (mol^{-1}); x_g = the mass susceptibility (g^{-1}); M_w = the molecular weight of the complex (g mol^{-1}); and x_{Di} = the diamagnetic correction (emu mol^{-1}).[6]

The magnetic moment μ_{eff} is then calculated using the following equation:

$$\mu_{eff} = 2.84\sqrt{x_m \cdot \mathrm{T}}$$

where: μ_{eff} = magnetic moment (B.M.); x_m = the molar susceptibility; and T = the absolute temperature (K).

The observed data are presented in Table S1 and as a Curie-Weiss plot in Fig. S4.

5. Magnetic susceptibility measurements of neat $[P_{4444}]_2[Co^{II}(Sal)_2]$

Experimental: Magnetic susceptibility measurements were performed using a Quantum Design SQUID magnetometer MPMS-XL housed at the Colorado State University, Fort Collins, Colorado. Measurements were performed on three different batches of neat $[P_{4444}]_2[Co^{II}(Sal)_2]$ samples with masses of 28.24, 87.84, and 55.22 mg, in the 1.8 to 310 K temperature range for *dc* applied magnetic fields of 0 to 5 T. The samples were sealed in a small low-density polyethylene bag and inserted in the sample holder straw. The magnetic data were corrected for the sample holder and the diamagnetic contributions of the compound using Pascal's constants. Prior to variable temperature experiments, the field-dependent magnetisation was measured at 100 K in order to detect the presence of any bulk ferromagnetic impurities. The perfect linearity found in the *M* vs. *H* plot at 100 K (Fig. S5) is consistent with the absence of ferromagnetic impurities.

Magnetic properties: The temperature dependence of magnetic susceptibility was measured at 1000 Oe between 1.8 and 310 K for 28.24 mg of sample. As shown in Fig. S6 (left), at 300 K the $\chi_M T$ product is 1.53 cm^3 K mol^{-1} Co(II), which is significantly higher than expected for a low spin (LS) Co(II) ion having total spin S = ½ and Landé factor g = 2 (theoretical Curie constant = 0.375 cm^3 K mol^{-1}), but also lower than predicted for a high spin (HS) S = 3/2 Co(II) ion (1.875 cm^3 K mol^{-1} expected). The $\chi_M T$ value decreases very gradually with temperature down to 35 K; this decrease is likely due to temperature independent paramagnetism. Below 35 K, $\chi_M T$ decreases more rapidly and reaches 0.89 cm^3 K mol^{-1} at 2 K; this is indicative of either antiferromagnetic interactions between Co(II) magnetic centers, or the presence of significant magnetic anisotropy in an S = 3/2 ion. To probe the spin state further, we measured the field dependence of the

magnetisation at 1.8 K (Fig. S6 (right)). We observe that the magnetisation is almost saturated at 5 T at a value of 1.08 μ_B, which is consistent with one unpaired electron per Co(II) ion (g = 2.16). However, the Brillouin "fit" of the M vs. H data at 1.8 K to an S = ½ model (Fig. S7) does not match the data. We conclude that a mononuclear model where all the Co(II) ions are magnetically equivalent is not consistent with the data.

In a possible "dinuclear" model, where two kinds of Co(II) ions are present in a 1:1 ratio, the re-plotted room temperature $\chi_M T$ value (Fig. S8 (left), 3.06 cm^3 K mol^{-1}) could match with one HS and one LS Co(II): the theoretical value is 3.05 cm^3 K mol^{-1} for g = 2.33, and $g > 2$ is expected for Co(II) in both HS and LS states. The corresponding M vs. H plot for this model (Fig. S8 (right)) reaches $M \sim 2.16$ μ_B at 5 T. To get one unpaired electron per Co(II) ion, either antiferromagnetic (AF) exchange coupling is operative to get total spin S = 1 at very low temperatures, or significant positive anisotropy of the HS Co(II) ion results in an effective S = ½ species at low temperatures. To rationalise two different Co(II) coordination environments, a one-dimensional array of Co(II) species (coordinative chain) can be proposed, with alternating HS and LS Co(II) units if the former are tetrahedral and the latter are octahedral (Fig. S9). Then, weak AF coupling between the Co(II) ions can reproduce the observed magnetic properties. Alternatively, a tetrahedral Co(II) center could show significant magnetic anisotropy, as has been observed previously,[7] thus obviating the need for exchange coupling.

Due to the liquid phase nature of the compound, it is very difficult to make an exact magneto-structural correlation, so the oligomeric chain proposed in Fig. S9 should be taken as one of several possible structures. Tetrahedral and square pyramidal Co(II) species are expected to be HS, octahedral species can be LS or HS depending on the nature of geometrical distortion, whereas square planar Co(II) should probably be LS, although HS has been observed in at least one case.[8] In the presence of an oxygen donor ligand, the Co(II) may hold an LS state as a hexacoordinated Co(II) complex with weak field ligands along the z-axis.[9] However, based on the magnetic data acquired and the presence of two bands in the visible electronic absorption spectrum (at 533 and 573 nm), we infer that the neat MCIL contains an approximate 1:1 mixture of HS and LS Co(II) complexes.

Phase transition study: Notable here, in the $\chi_M T$ vs. T plot (Fig. S6 (left)), no phase transition was observed above 270 K as observed in the DSC data. To study the possible phase transition behaviour in more detail, $\chi_M T$ data for two cycles of heating and cooling were collected in the temperature range 140–310 K (Fig. S10): these data exhibit no phase transition phenomenon.

Note on measurement reproducibility: The $\chi_M T$ vs. T plots of three different batches of samples ((a) 28.24 mg, (b) 87.84 mg, and (c) 55.22 mg) are found to be qualitatively similar, but not superimposable (Fig. S11). The major differences in these three different batches are: (i) amount of sample; and (ii) cooling rates: samples (a) and (b) were installed directly into the MPMS at 100 K, thus forcing very fast cooling from room temperature; whereas sample (c) was loaded into the instrument at 280 K and cooled to 2 K at a rate of 10 K min^{-1} before the data collection. Possible

explanations for the differences that we can conceive are as follows. (i) When a larger amount of sample is measured ((b) 87.84 mg) there is possible torqueing of the sample (more likely for the non-crystalline morphology of IL) which allows easier aligning of magnetic centers along the applied filed to produce a larger magnetisation response. (ii) If the morphology of the sample is not independent of the rate of cooling/heating, we might expect that the magnetic responses will not be exactly the same.

6. Thermo-physical properties of $[P_{4444}]_2[Co^{II}(Sal)_2]$

The thermo-physical properties of neat $[P_{4444}]_2[Co^{II}(Sal)_2]$ were determined by TGA and DSC measurements. TGA studies were performed under an N_2 atmosphere using a temperature ramp rate of 10 °C min^{-1}. Interpretation of the obtained TGA curve revealed that $[P_{4444}]_2[Co^{II}(Sal)_2]$ has fairly good thermal stability (T_{decomp} = 264 °C, Fig. S12). During the DSC heating process, an endothermic peak typical of a glass transition was observed at −45 °C (Fig. S13). In addition to this glass transition, a distinct endothermic peak was seen at 5 °C upon heating. In the DSC data of the MCIL after mixing with two equivalent of water molecules per one ion pair, such an endothermic peak was not observed, but typical recrystallisation/melting peaks were seen (Fig. S14). There are multiple possibilities for this endothermic phase transition, including spin crossover,[10] geometrical isomerisation,[11] valence tautomerism[12] of the Co(II) ion or melting of the MCIL from a super-cooled state. Although the LS state rules out a spin-crossover event, the temperature-dependent solution magnetic moment value was examined for evidence of valence tautomerism. During the variable-temperature NMR experiments, a distinct colour change was observed and associated with a change in the Curie constant at approximately −20 °C (Fig. S4). The underlying cause for these changes in both the Curie constant and the colour of $[P_{4444}]_2[Co^{II}(Sal)_2]$ in dichloromethane has not been determined yet. Detailed investigations on this topic are currently underway.

Variable-temperature PLM and regular optical microscopy studies of the MCIL were then undertaken to analyse the phase transition observed during thermal analysis. PLM study revealed the MCIL existed as an isotropic phase (Fig. S15). Fig. S16 shows microscopy images of the MCIL with an air bubble at temperatures before and after the endothermic phase transition. The air bubble did not move even after applying pressure at 0 °C, but started to move with pressure at 10 °C. In addition, no colour change was seen within the temperature range. Given the aforementioned results, the endothermic phase transition seen at 5 °C should be melting of $[P_{4444}]_2[Co^{II}(Sal)_2]$ without recrystallisation prior to melting.

7. Equilibrium binding study of $[P_{4444}]_2[Co^{II}(Sal)_2]$ with water, methanol, and ethanol

The equilibrium between four-coordinate $[P_{4444}]_2[Co^{II}(Sal)_2]$ to its six-coordinate $[P_{4444}]_2[Co^{II}(Sal)_2(solv.)_2]$ form upon addition of two molar equivalents of a solvent (solv.) can be described as follows:

$$[P_{4444}]_2[Co^{II}(Sal)_2] + 2Solv. \underset{\leftarrow}{\overset{\rightarrow}{}} [P_{4444}]_2[Co^{II}(Sal)_2(Solv.)_2]$$

To calculate the equilibrium constant (K_{eq}) of the above solvent-binding equilibrium for the neat $[P_{4444}]_2[Co^{II}(Sal)_2]$ MCIL, the ratio of six-coordinate to four-coordinate complexes (K)[13] was first calculated by adding differing amounts of the solvent molecules to the system as described in the following equations:

$$A = \varepsilon_{six}[Co]_{six} + \varepsilon_{four}[Co]_{four}$$

$$[Co]_{six} = K \cdot [Co]_{four}$$

$$[Co]_{four} = (1-K) \cdot [Co]_t$$

where: A = the UV-visible absorbance of the $[P_{4444}]_2[Co^{II}(Sal)_2]$/solvent mixture; ε_{six} = the extinction coefficient of he six-coordinate complex (ε_{six} = 1.3); ε_{four} = the extinction coefficient of four-coordinate complex (ε_{four} = 138); $[Co]_{six}$ = the concentration of six-coordinate complex (M units); $[Co]_{four}$ = the concentration of four-coordinate complex (in M units); $[Co]_t$ = the total concentration of the complex (in M units); and K = the molar ratio of six-coordinate to four-coordinate complex. (Note that total volume of the mixture was approximated by calculating the sum of the mixed volumes of the IL and solvents.) The ε_{four} value was calculated by measuring both absorbance and density of neat $[P_{4444}]_2[Co^{II}(Sal)_2]$. The absorbance of the neat MCIL was measured by a demountable quartz cuvette with a path length of 0.1 mm at 30 °C. The density of the MCIL was measured by carefully filling 1.00-mL volumetric flask with the MCIL and the mass of the filled flask was recorded, and the mass of the empty flask was subtracted. The difference in mass gave the density to be 1.05 (g cm^{-3}). The concentration of neat MCIL was then calculated to be 1.24 M, and the absorbance of neat MCIL was divided by the concentration, which gave the value of ε_{four}. The ε_{six} value was also determined by measuring the absorbance of a dilute MCIL solution in methanol (10 mM), in which all MCIL is expected to become the six-coordinate complex with two Co(II)-bound solvent molecules.

The equilibrium constant K_{eq} (M^{-2}) value at which 2 molar equivalents of a solvent were mixed with the MCIL was then calculated using following equation:

$$K_{eq} = \frac{[Co]_{six}}{[Co]_{four}[Solv.]^2}$$

Binding equilibria of $[P_{4444}]_2[Co^{II}(Sal)_2]$ with water, methanol, and ethanol were also studied with the MCIL as an acetonitrile solution. Acetonitrile was chosen because it acts as a good solvent for all components. To study the binding equilibria of each solvent, a 25-mL stock solution of

$[P_{4444}]_2[Co^{II}(Sal)_2]$ was prepared in dry acetonitrile at a concentration of approximately 0.018 M. A reference value for the UV-visible absorbance of $[P_{4444}]_2[Co^{II}(Sal)_2]$ was obtained by using a 1-mL aliquot of the stock solution. The binding studies were performed by: calculating the amount of binding solvent to add to the solution, adding that amount of binding solvent, shaking the resulting solution and then taking a 1-mL aliquot and collecting the UV-visible spectrum. This process was repeated until the desired number of data points had been collected. The equilibrium constants were calculated by using the same equation above.

8. Coordination selectivity of $[P_{4444}]_2[Co^{II}(Sal)_2]$ after mixing with a liquid-state water/alcohol mixture

Selective coordination of water molecules $[P_{4444}]_2[Co^{II}(Sal)_2]$ from alcohols (methanol and ethanol) was demonstrated by Infrared spectra. Both bending vibration O-H band (δ(OH); Fig. S24 upper right) and stretching M-O band (ν(MO); Fig. S24 bottom left) were observed when two water molecules were added to $[P_{4444}]_2[Co^{II}(Sal)_2]$. These bands are assigned to coordinated water molecules. Upon mixing both methanol and ethanol, a stretching O-H band (ν(OH); Fig. S24 upper left) was seen around 3200~3500 cm^{-1}, and stretching C-O band (ν(CO); Fig. S24 bottom left) was seen around 1200 cm^{-1}. This suggests both alcohols are dissolved in but does not coordinate to $[P_{4444}]_2[Co^{II}(Sal)_2]$. Upon mixing excess amount of alcohols (ten molar equivalents), broad ν(OH) was seen around 1350~1280 cm^{-1} (Fig. S24 bottom right). These bands are distinct from that of coordinated water. The typical bands derived from coordinated water molecules were also seen when both water and alcohol molecules were added to $[P_{4444}]_2[Co^{II}(Sal)_2]$ at the same time (Fig. S24 upper right and bottom left). This clearly shows that $[P_{4444}]_2[Co^{II}(Sal)_2]$ selectively coordinates water even in the presence of these alcohols.

9. ATIR-FTIR measurement on $[P_{4444}]_2[Co^{II}(Sal)_2]$ after exposure to a water/alcohol vapour mixture

An equal volume of both water and alcohols (methanol or ethanol) were mixed (500 mL/500 mL) and were loaded in 1-L Bucher flask with vigorous stirring. The argon gas was passed through the mixed solvent, and the resulting mixed vapour gas was bubbled through 100 mg of MCIL with stirring for 5 minutes. The resulting mixture was placed in vacuo to remove the residual solvents. ATR-FTIR measurements were undertaken for the MCIL before and after removing the solvents. ATR-FTIR data show that typical bands assigned to coordinated water molecules were seen after bubbling water/alcohol mixed argon gas (Fig. S25). ν(CO) FTIR bands characteristic of unbound alcohols were also observed, suggesting that both methanol and ethanol vapours are dissolved in but do not bind to $[P_{4444}]_2[Co^{II}(Sal)_2]$. Upon evacuation of the mixture, no IR band from the coordinated water was seen in the spectra. The above results and data are consistent with $[P_{4444}]_2[Co^{II}(Sal)_2]$ selectively and reversibly coordinating water vapour in the presence of alcohol vapour.

Supporting Tables and Figures

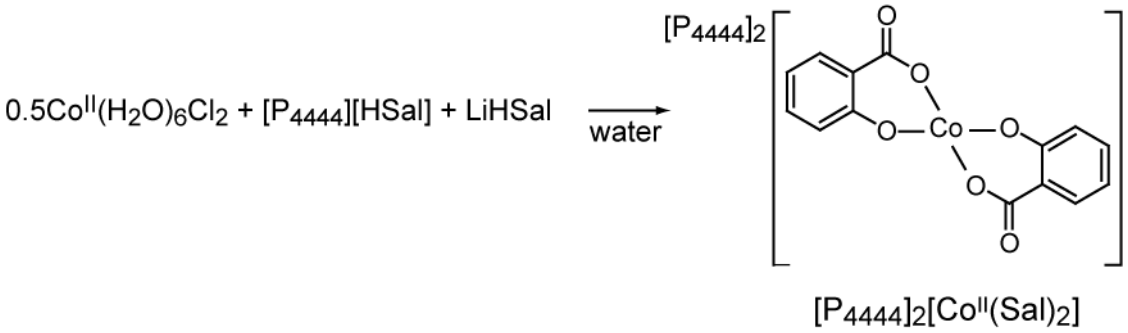

Scheme S1 Preparation of a cobalt(II) bis(salicylate)-based MCIL ([P_{4444}]$_2$[Co^{II}(Sal)$_2$]).

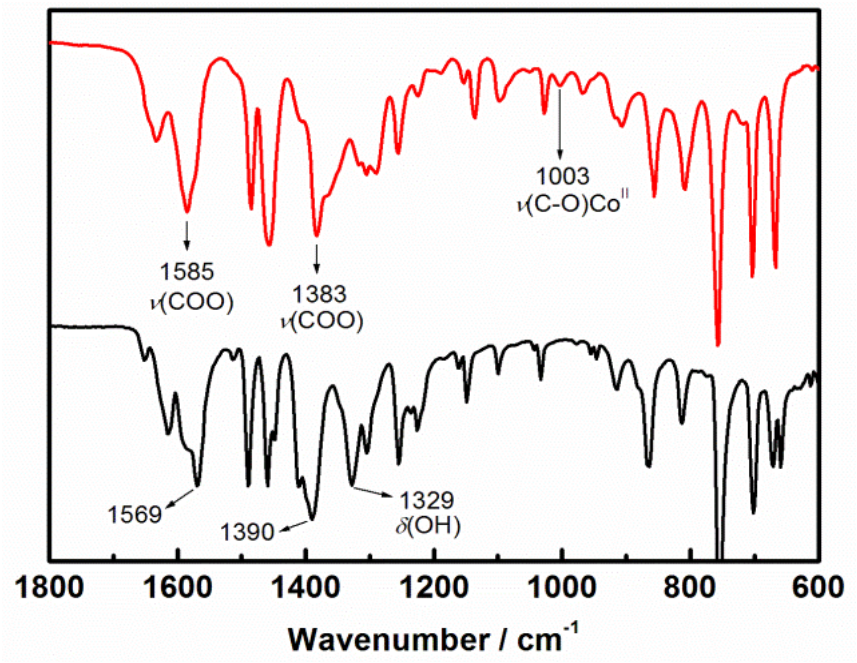

Fig. S1 Infrared spectra of [P_{4444}]$_2$[Co^{II}(Sal)$_2$] (red line) and LiHSal (black line). The phenolic O-H bending mode (δ(OH)) disappeared, and a new stretching vibration mode assigned to ν((C–O)M)[14] was observed. In addition, asymmetric stretching vibration of carboxylate group (ν_{as}(COO−)) was shifted to higher wavenumber (1569 to 1585 cm^{-1}), and symmetric stretching vibration of the carboxylate group (ν_s(COO−)) was shifted to lower wavenumber (1390 to 1383 cm^{-1}) as compared to those of LiHSal. These results are concordant with other complexes where the salicylate anion acts as a bidentate ligand.[15]

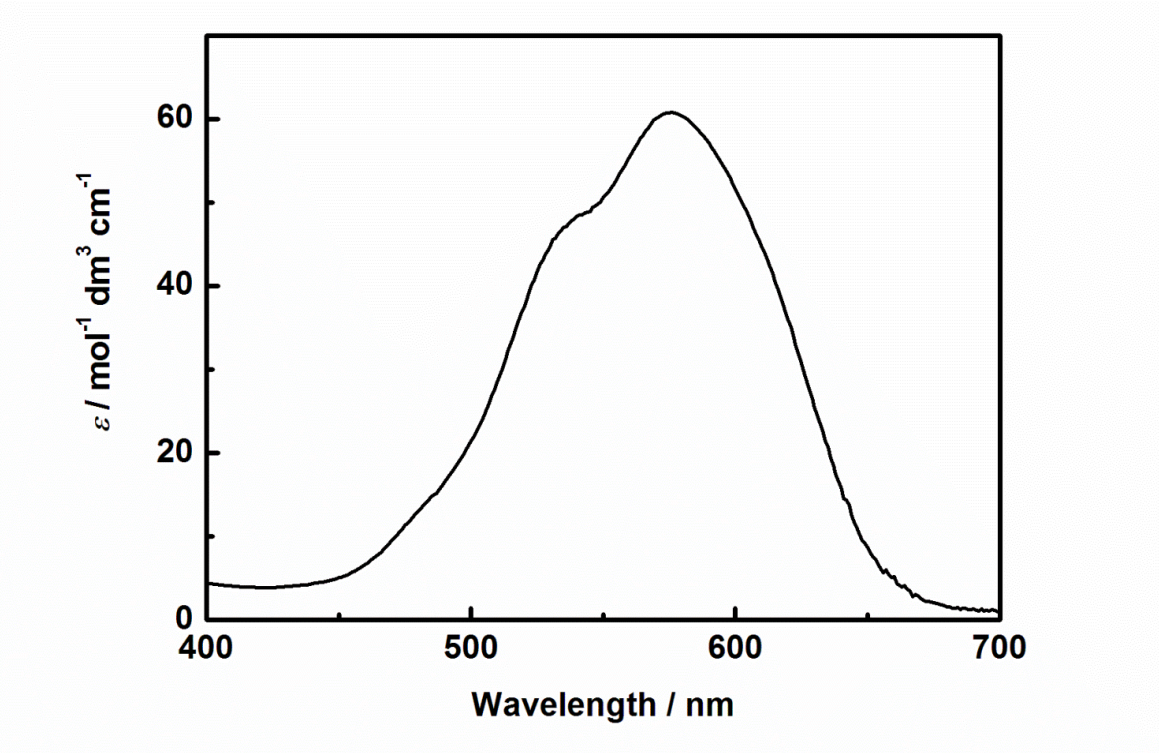

Fig. S2 UV-visible spectrum of $[P_{4444}]_2[Co^{II}(Sal)_2]$ in dichloromethane (10 mM). Two distinct bands at 533 (ε = 48) and 573 (ε = 63 units) nm were observed.

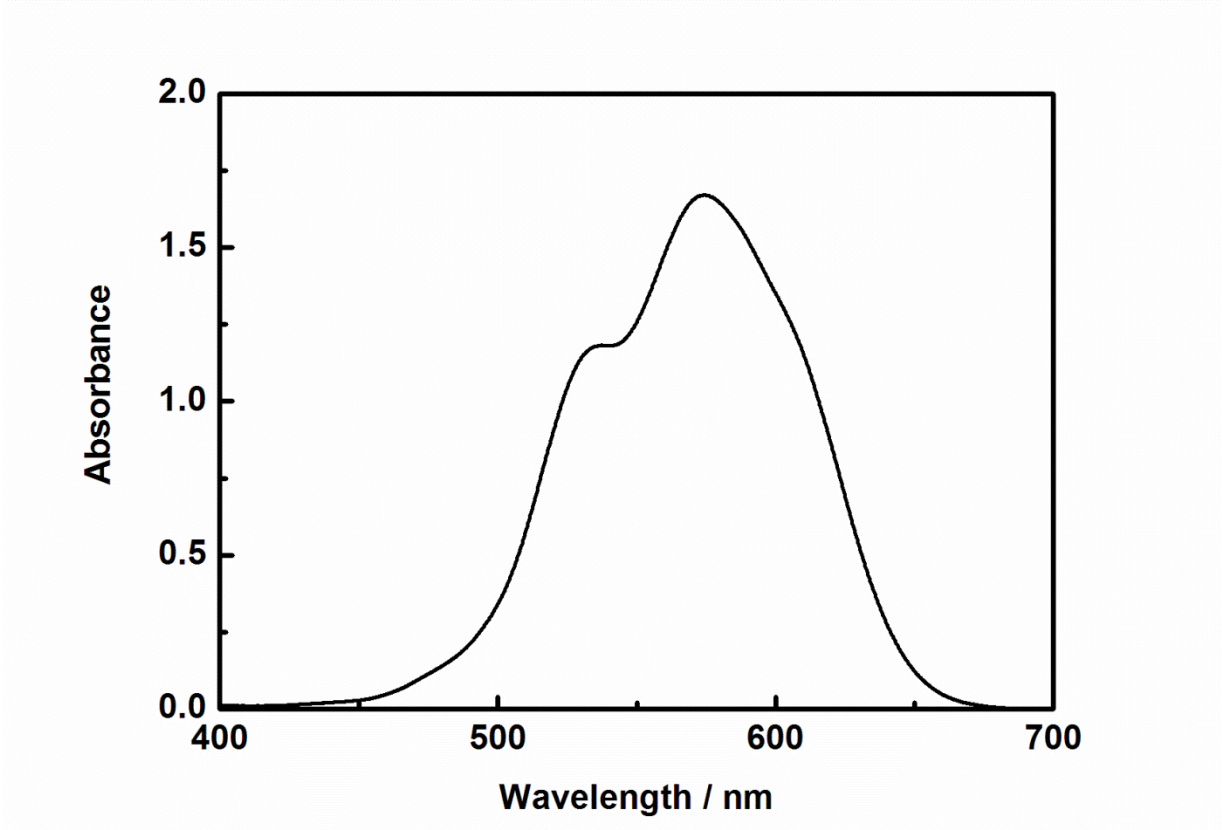

Fig. S3 UV-visible spectrum of neat $[P_{4444}]_2[Co^{II}(Sal)_2]$ in a demountable quartz cell with a path length of 0.1 mm.

Table S1 The magnetic moment and magnetic susceptibility (χT) values of $[P_{4444}]_2[Co^{II}(Sal)_2]$ as determined by the Evans method.

Temperature (K)	Magnetic Moment (Bohr magnetons (μ_B))	χT
293	2.13	0.56
178	2.73	0.92
198	2.66	0.88
218	2.58	0.82
238	2.50	0.78
258	2.38	0.70
278	2.29	0.65
298	2.15	0.57

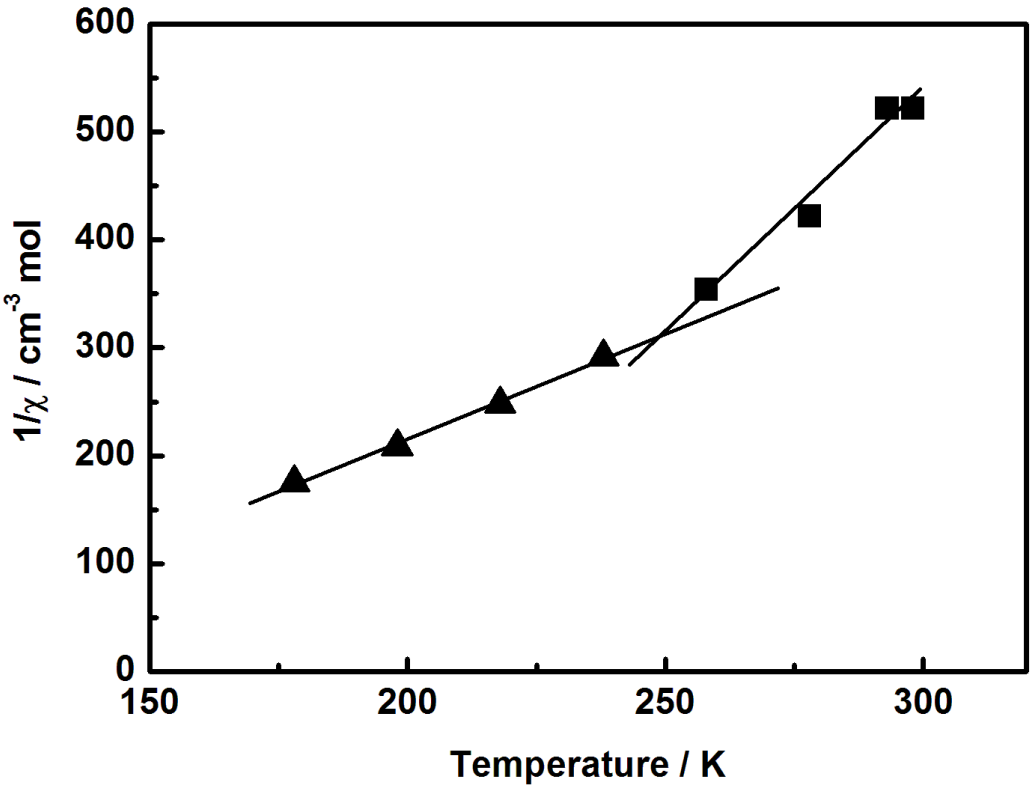

Fig. S4 Plot of inverse magnetic susceptibility vs. temperature for neat $[P_{4444}]_2[Co^{II}(Sal)_2]$. The data points collected at the two different temperature regimes are denoted by triangles and squares.

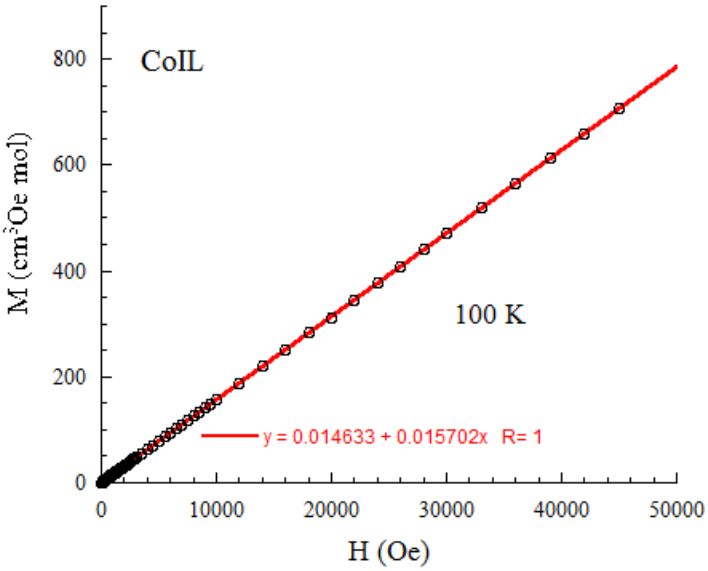

Fig. S5 The linear fit of the $M = f(H)$ data at 100 K for neat $[P_{4444}]_2[Co^{II}(Sal)_2]$.

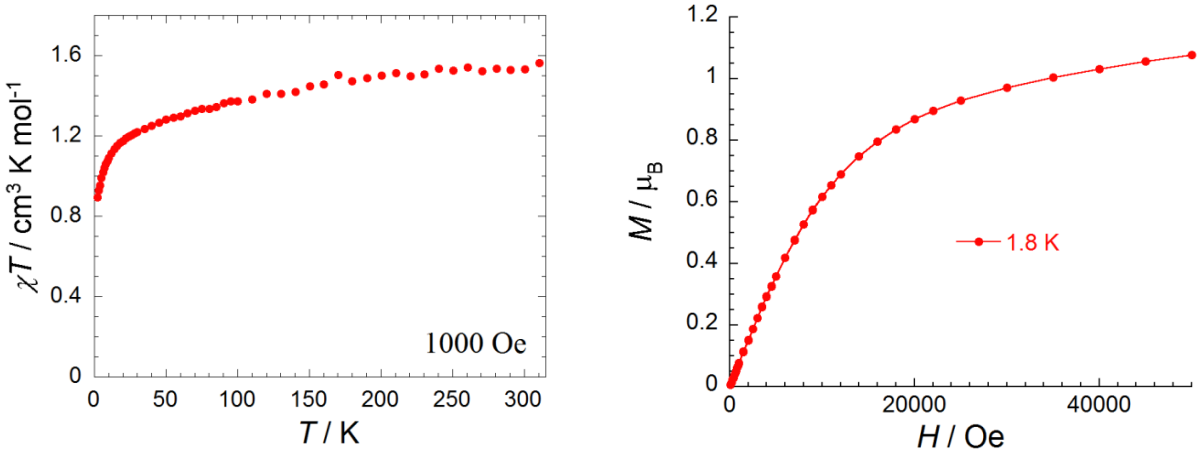

Fig. S6 Plots of $\chi_M T$ vs. T plot at 1000 Oe (left) and M vs. H data at 1.8 K (right) for neat $[P_{4444}]_2[Co^{II}(Sal)_2]$. A mononuclear Co(II) species is assumed here.

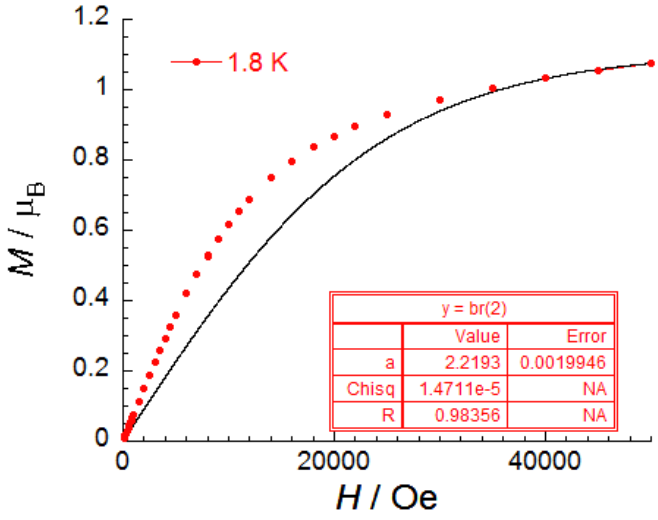

Fig. S7 Brillouin fit of M vs. H data at 1.8 K with $S = 1/2$ spin for neat $[P_{4444}]_2[Co^{II}(Sal)_2]$. The solid red circles are the experimental data points, and the solid black line is the Brillouin fit of the data. This fit displays almost no correspondence to the experimental data (only a few very high field data points correlate with the fit).

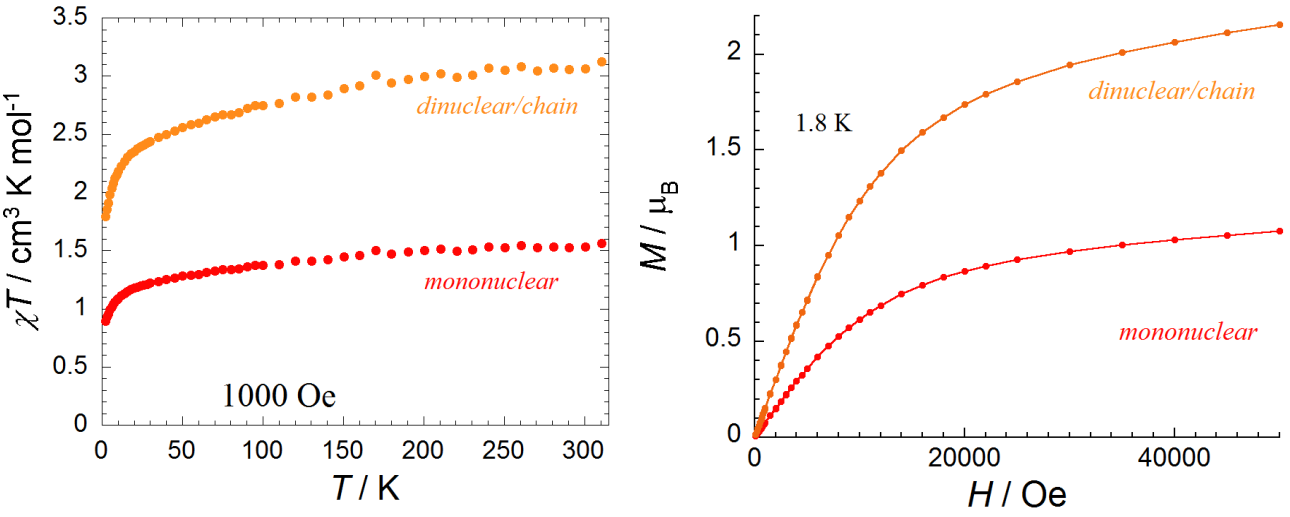

Fig. S8 Comparative plots for the mononuclear and dinuclear/chain models for neat $[P_{4444}]_2[Co^{II}(Sal)_2]$: $\chi_M T$ vs. T at 1000 Oe (left); M vs. H data at 1.8 K (right).

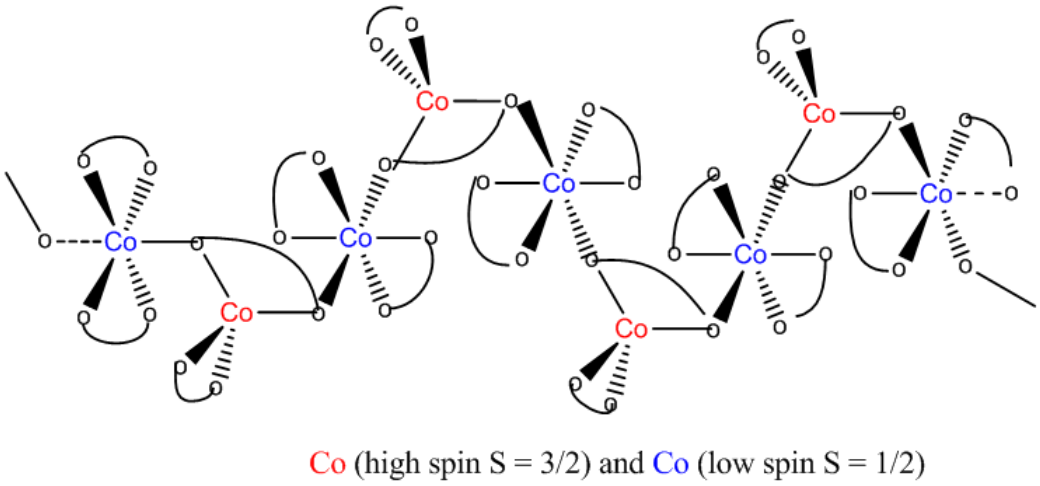

Fig. S9 A schematic representation of a structure of neat $[P_{4444}]_2[Co^{II}(Sal)_2]$ consistent with initial magnetic susceptibility studies: a one-dimensional coordination oligomer with alternating tetrahedral HS and octahedral LS Co(II) units.

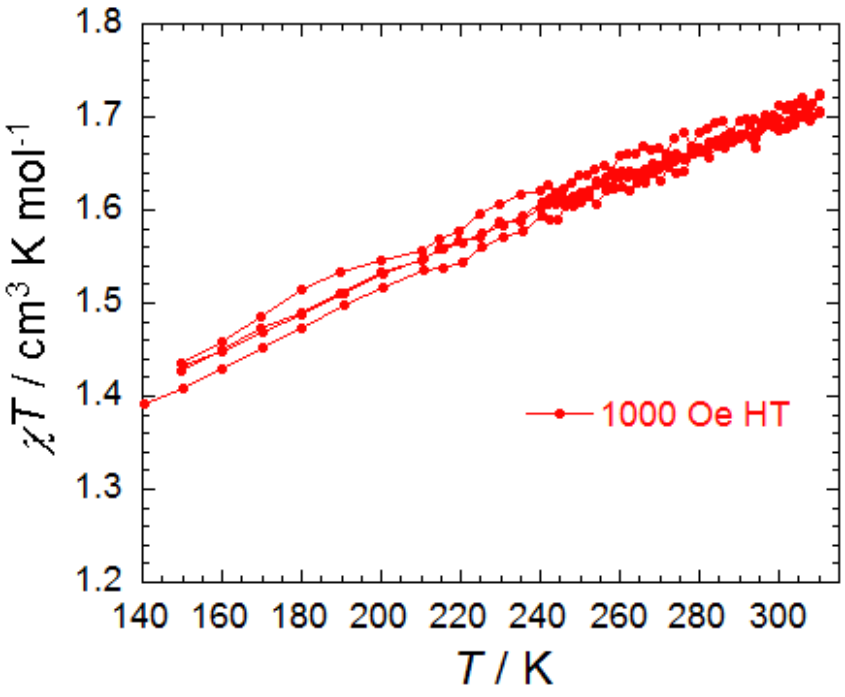

Fig. S10 The $\chi_M T$ vs. T plot at 1000 Oe for neat $[P_{4444}]_2[Co^{II}(Sal)_2]$ with two heating and cooling cycles between 140 and 310 K. The solid red circles are the experimental data, and the red lines are guidelines connecting successive data points in the heating and cooling runs.

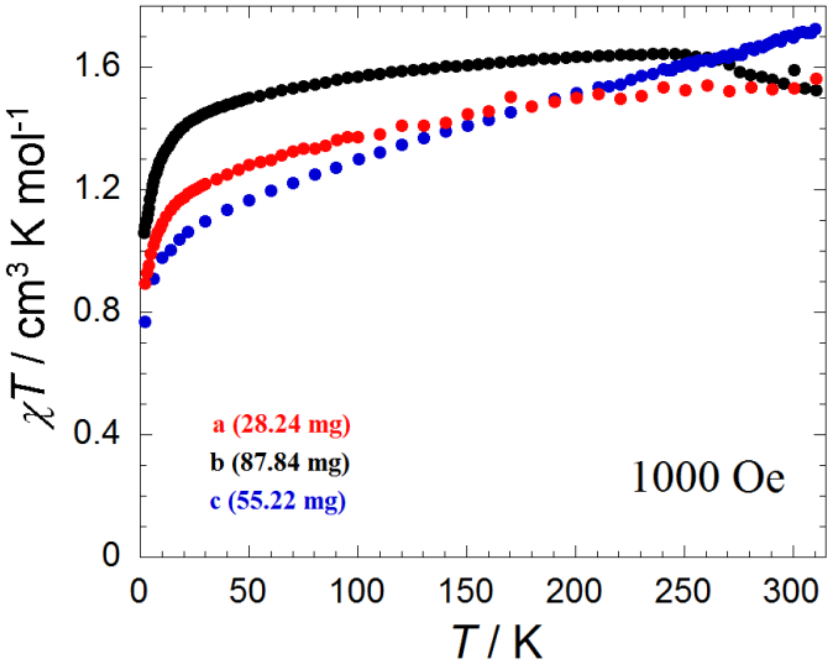

Fig. S11 The $\chi_M T$ vs. T plots at 1000 Oe for neat $[P_{4444}]_2[Co^{II}(Sal)_2]$ for three different mass samples: (a) 28.24 mg (red), (b) 87.84 mg (black), and (c) 55.22 mg (blue).

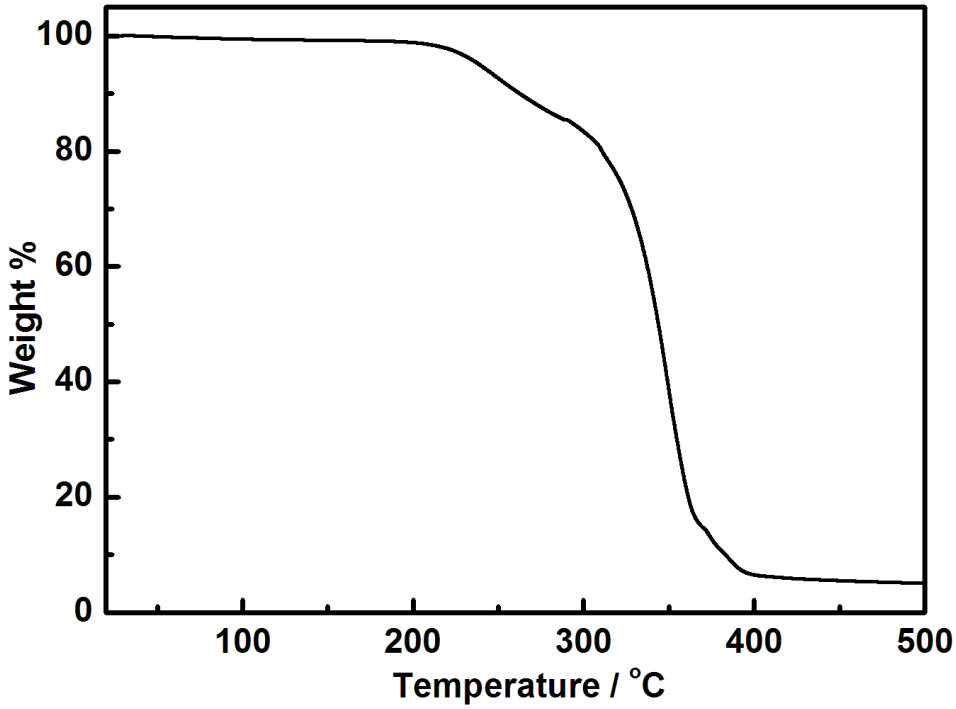

Fig. S12 TGA profile of $[P_{4444}]_2[Co^{II}(Sal)_2]$ under N_2 with a temperature ramp rate of 10 °C min^{-1}. The thermal decomposition temperature (T_{decomp}) was determined as the temperature at which 10% mass loss of the sample occurred.

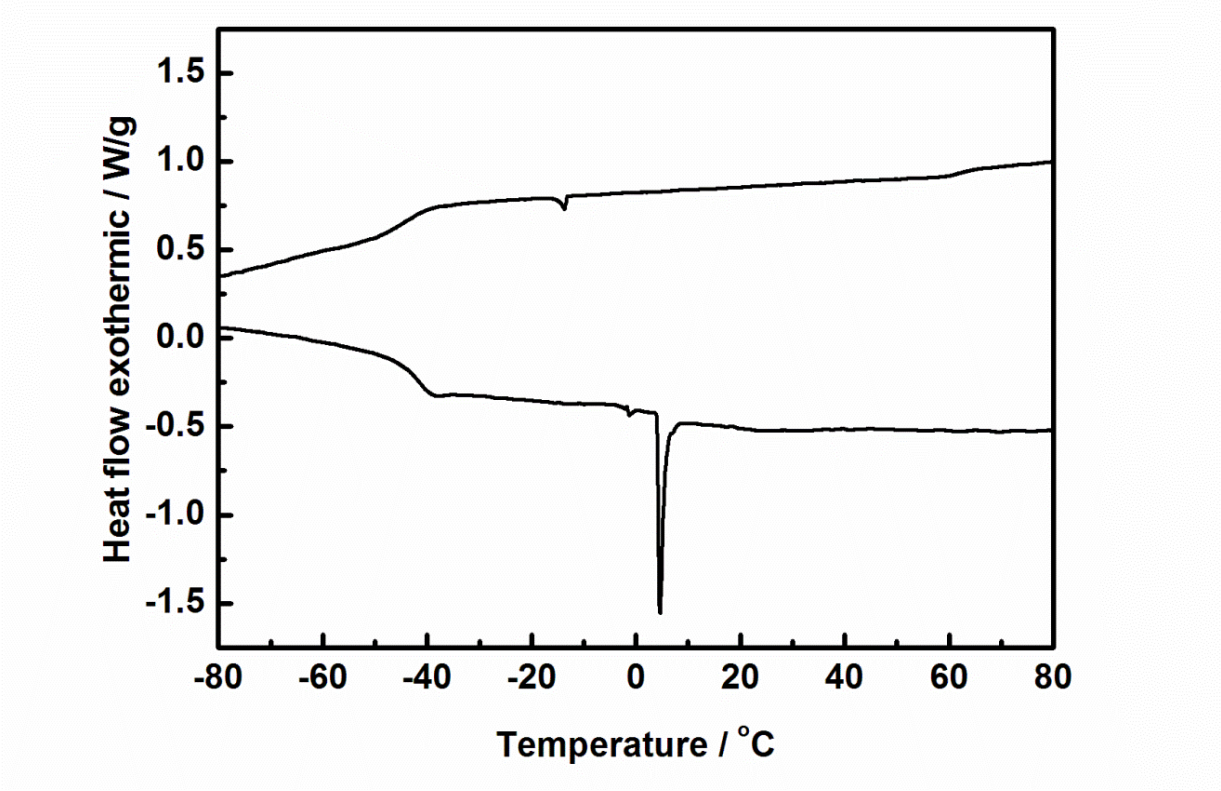

Fig. S13 DSC profile of neat $[P_{4444}]_2[Co^{II}(Sal)_2]$ with a temperature ramp rate of 5 °C min^{-1}.

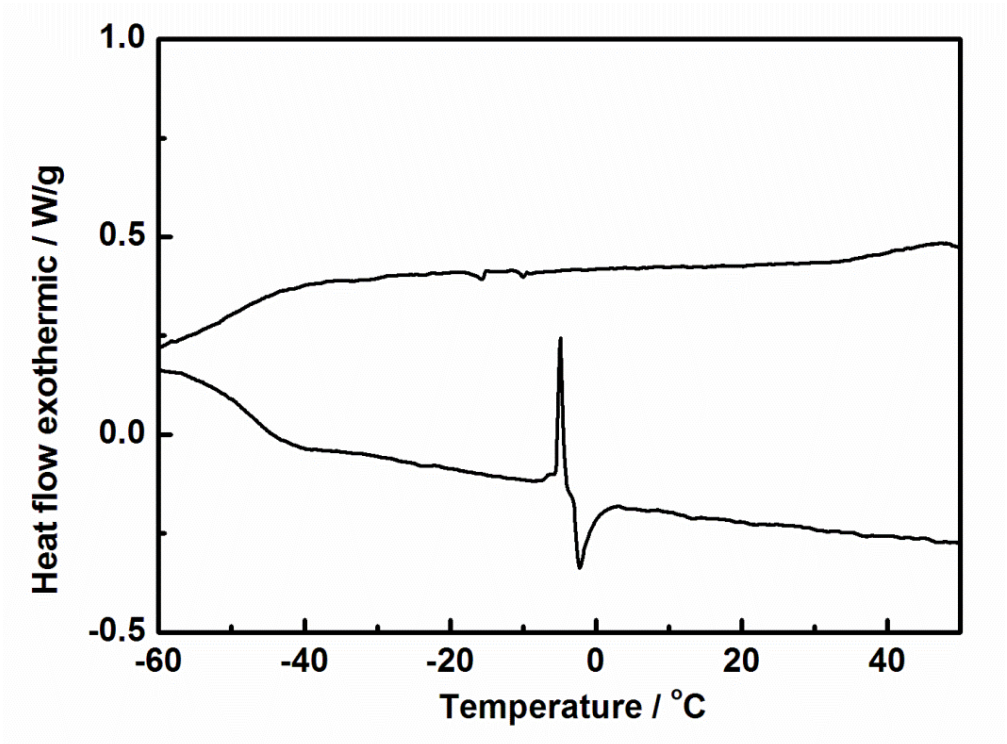

Fig. S14 DSC profile of $[P_{4444}]_2[Co^{II}(Sal)_2]$ after mixing with two equivalents of water. Temperature ramp rate = 5 °C min^{-1}.

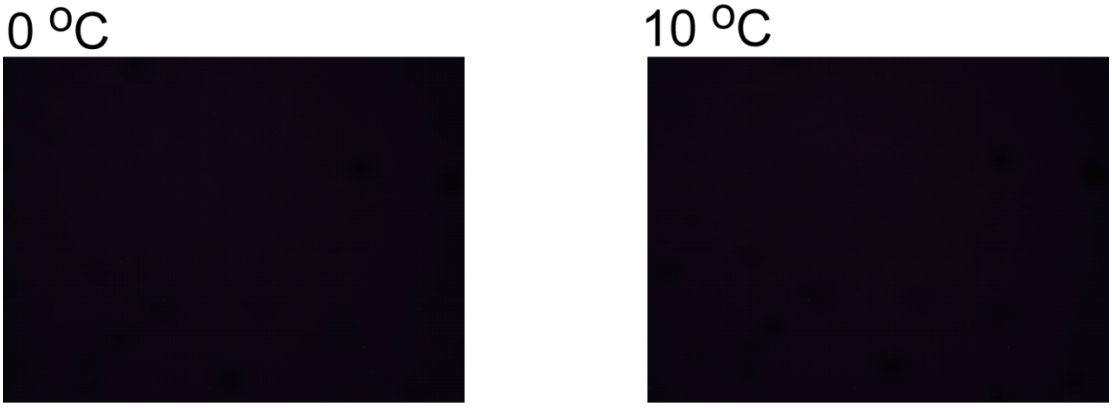

Fig. S15 PLM images of $[P_{4444}]_2[Co^{II}(Sal)_2]$ before and after the phase transition observed by DSC at ca. 5 °C.

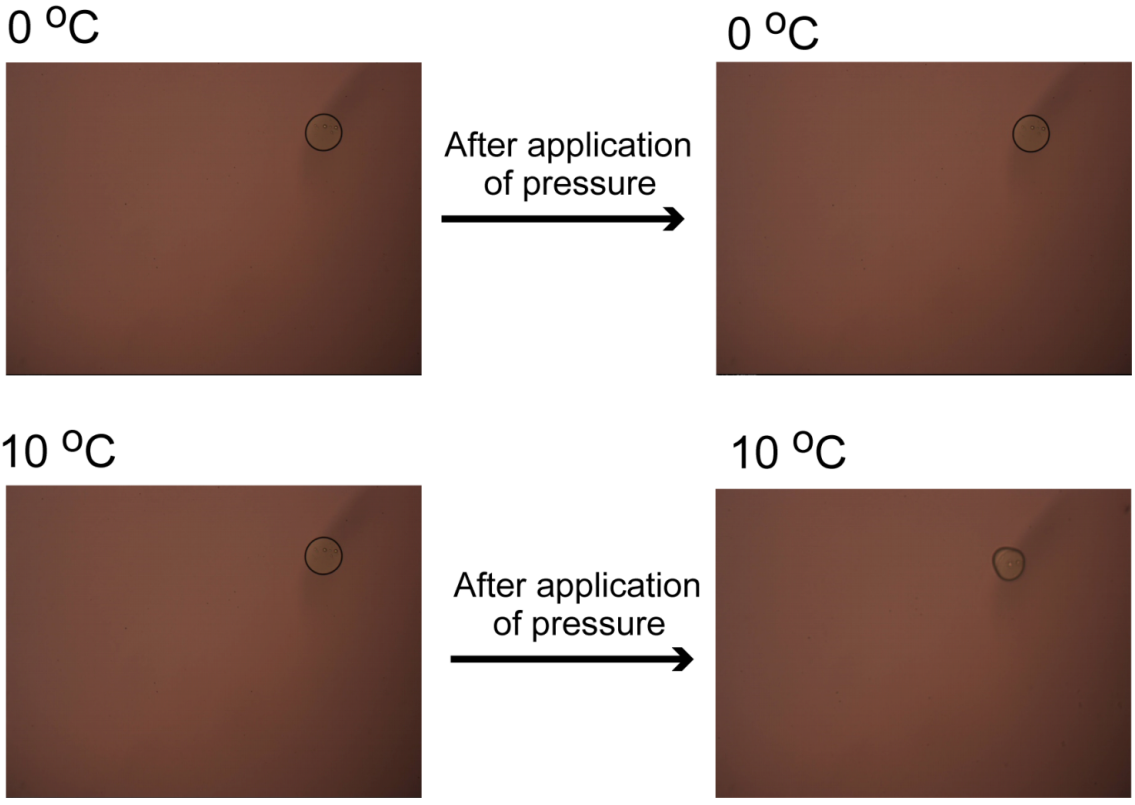

Fig. S16 Microscopy images of $[P_{4444}]_2[Co^{II}(Sal)_2]$ before and after the observed DSC phase transition at ca. 5 °C. A circle object seen in the image is an air bubble.

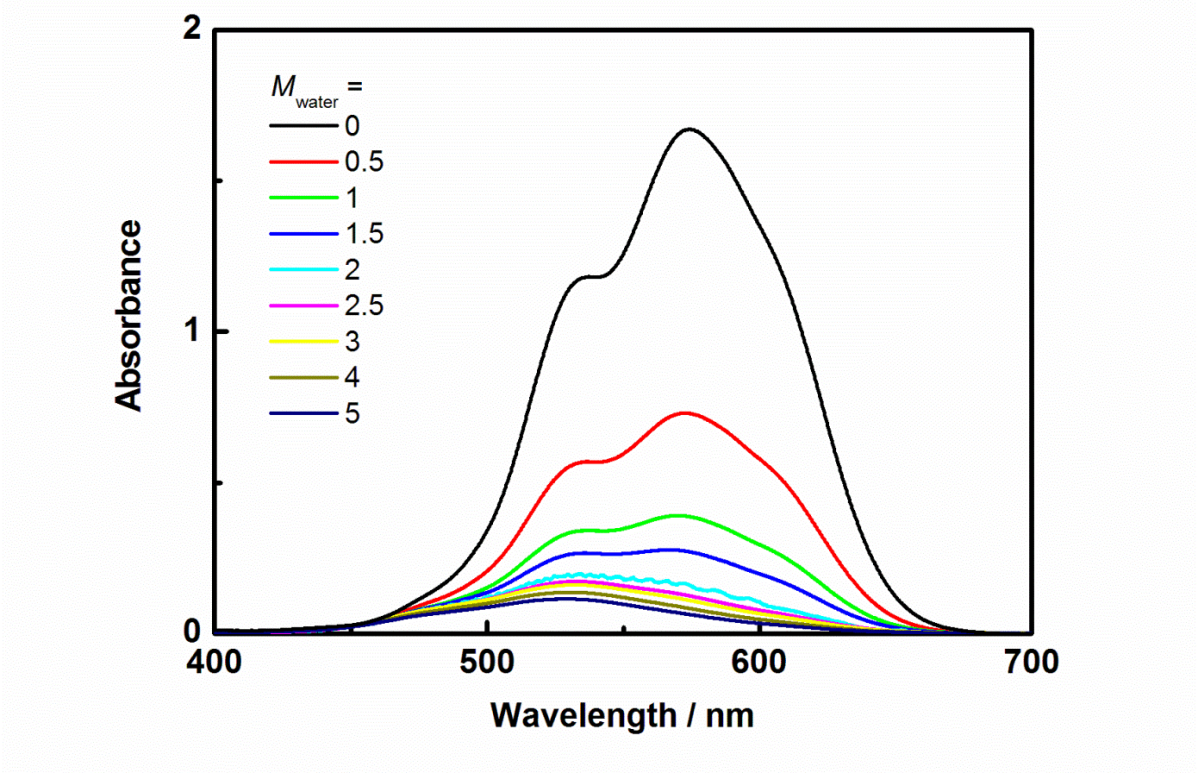

Fig. S17 UV-visible spectra of $[P_{4444}]_2[Co^{II}(Sal)_2]$ after mixing with different amounts of water (M_{water} = 0 to 5.0).

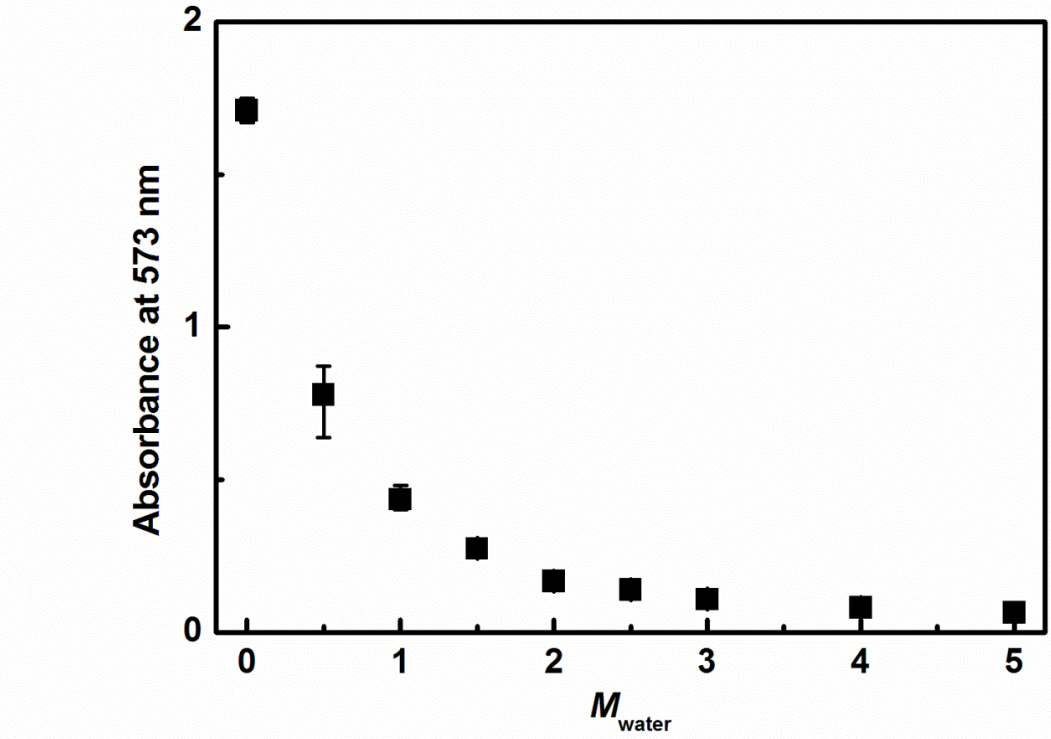

Fig. S18 The absorbance at 573 nm of $[P_{4444}]_2[Co^{II}(Sal)_2]$ after mixing with different amounts of water molecules per ion pair (M_{water} = 0 to 5.0).

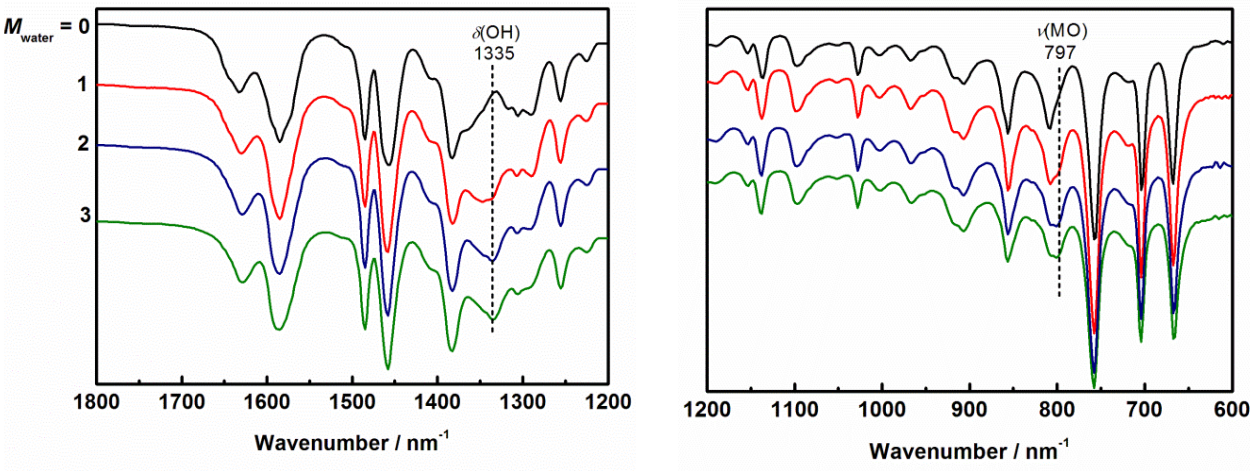

Fig. S19 ATR-FTIR spectra of $[P_{4444}]_2[Co^{II}(Sal)_2]$/water mixtures with M_{water} values from 0 to 3.0.

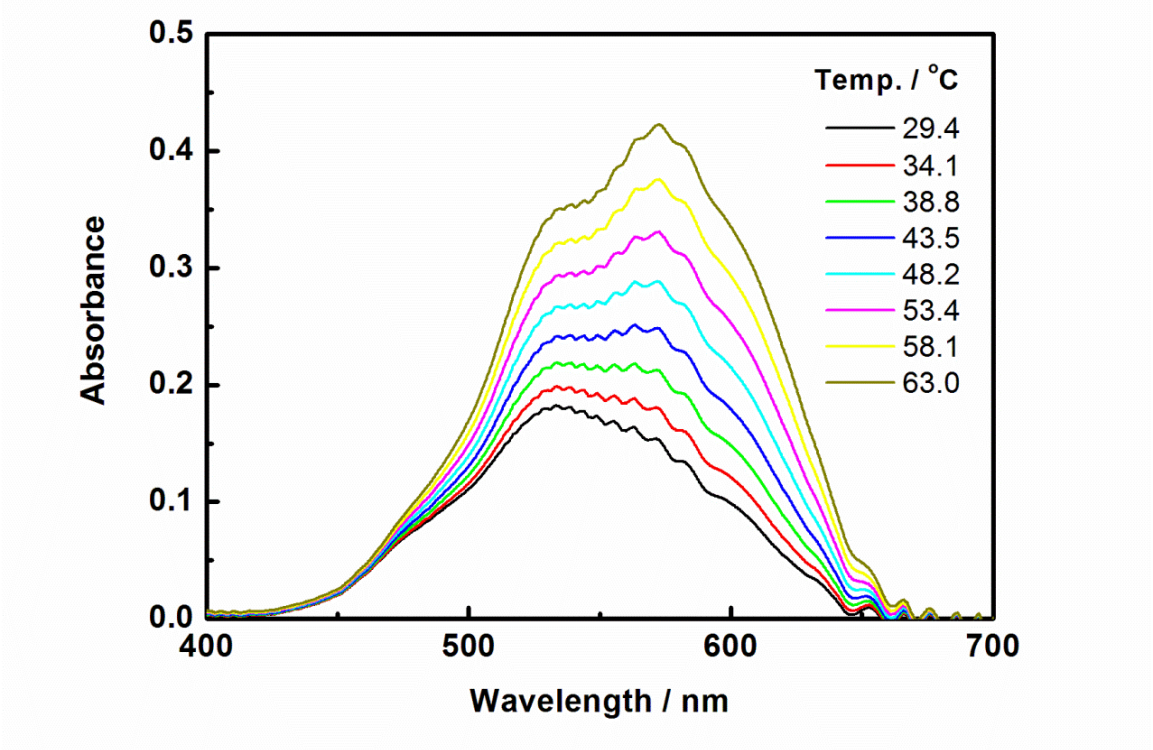

Fig. S20 UV-visible spectra of a M_{water} = 2.0 $[P_{4444}]_2[Co^{II}(Sal)_2]$/water mixture upon heating.

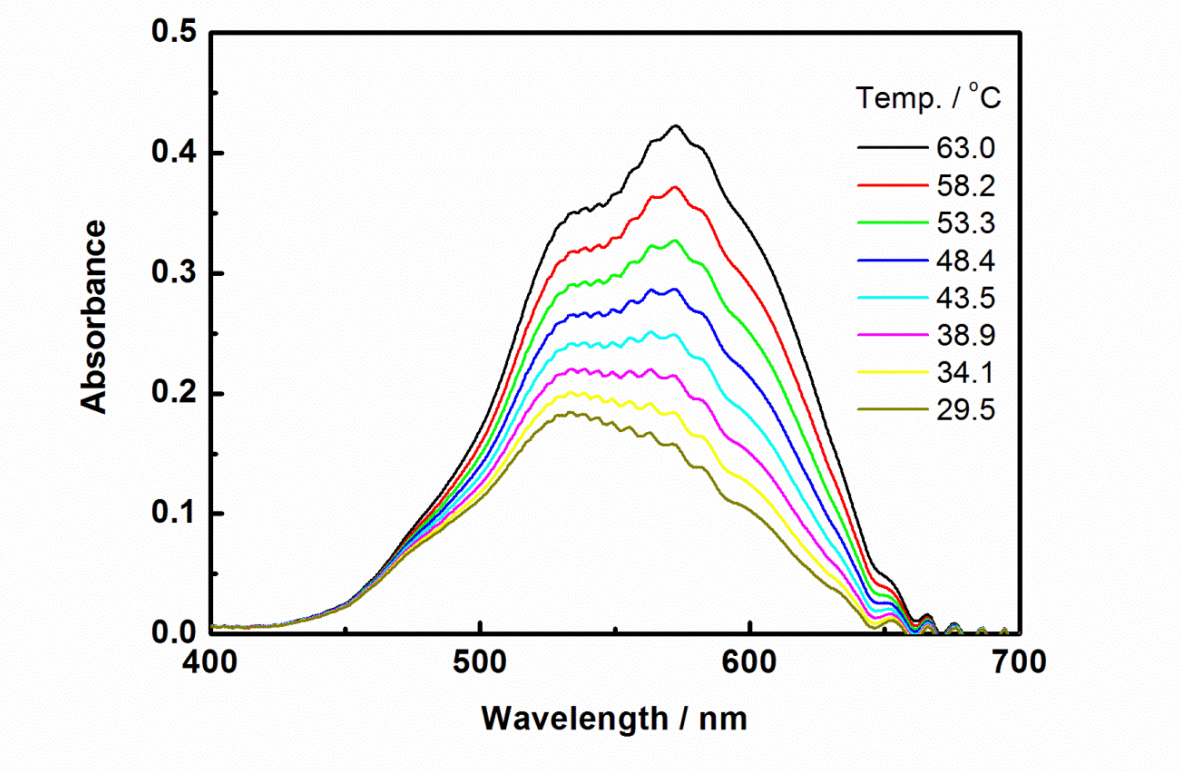

Fig. S21 UV-visible spectra of a M_{water} = 2.0 $[P_{4444}]_2[Co^{II}(Sal)_2]$/water mixture upon cooling.

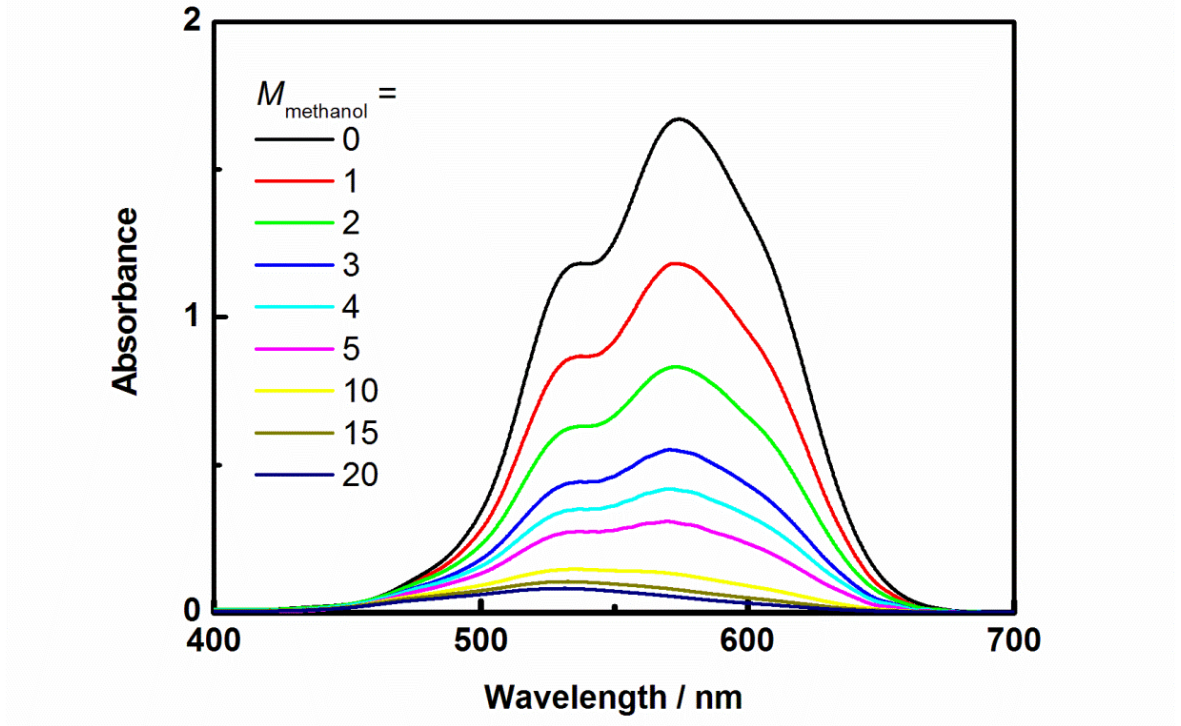

Fig. S22 UV-visible spectra of $[P_{4444}]_2[Co^{II}(Sal)_2]$ after mixing with different amounts of methanol ($M_{methanol}$ = 0 to 20).

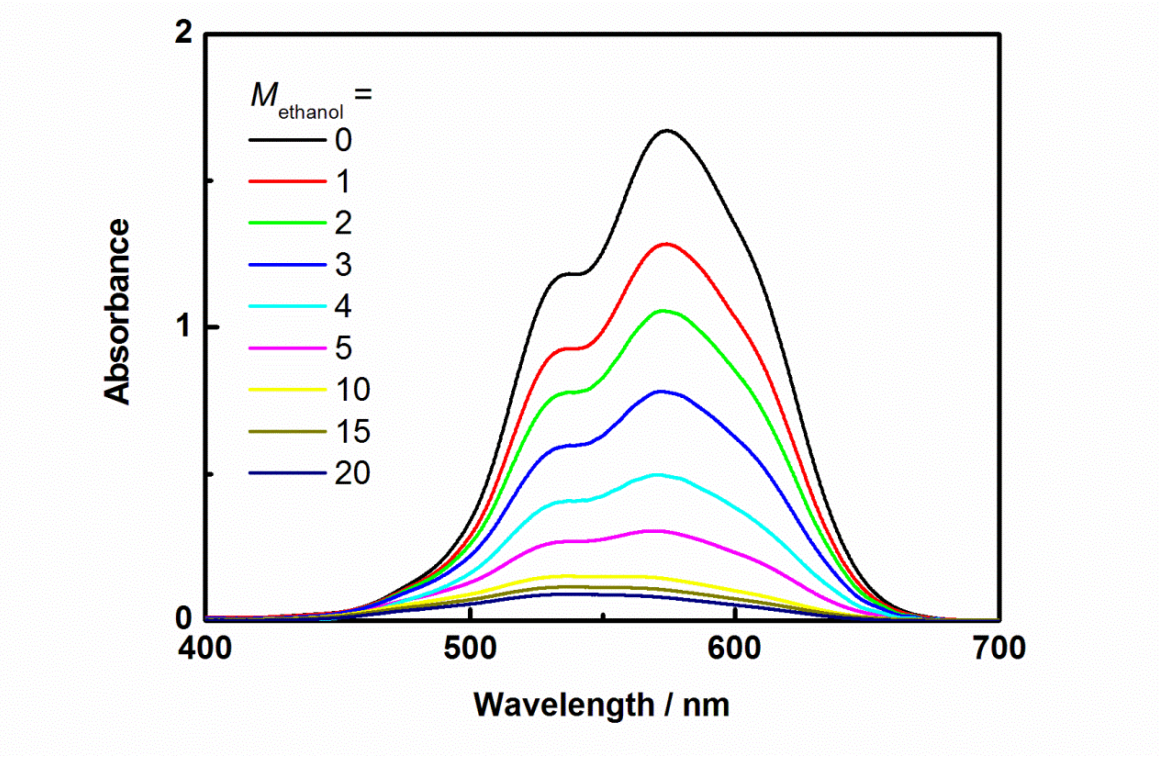

Fig. S23 UV-visible spectra of $[P_{4444}]_2[Co^{II}(Sal)_2]$ after mixing with different amounts of ethanol ($M_{ethanol}$ = 0 to 20).

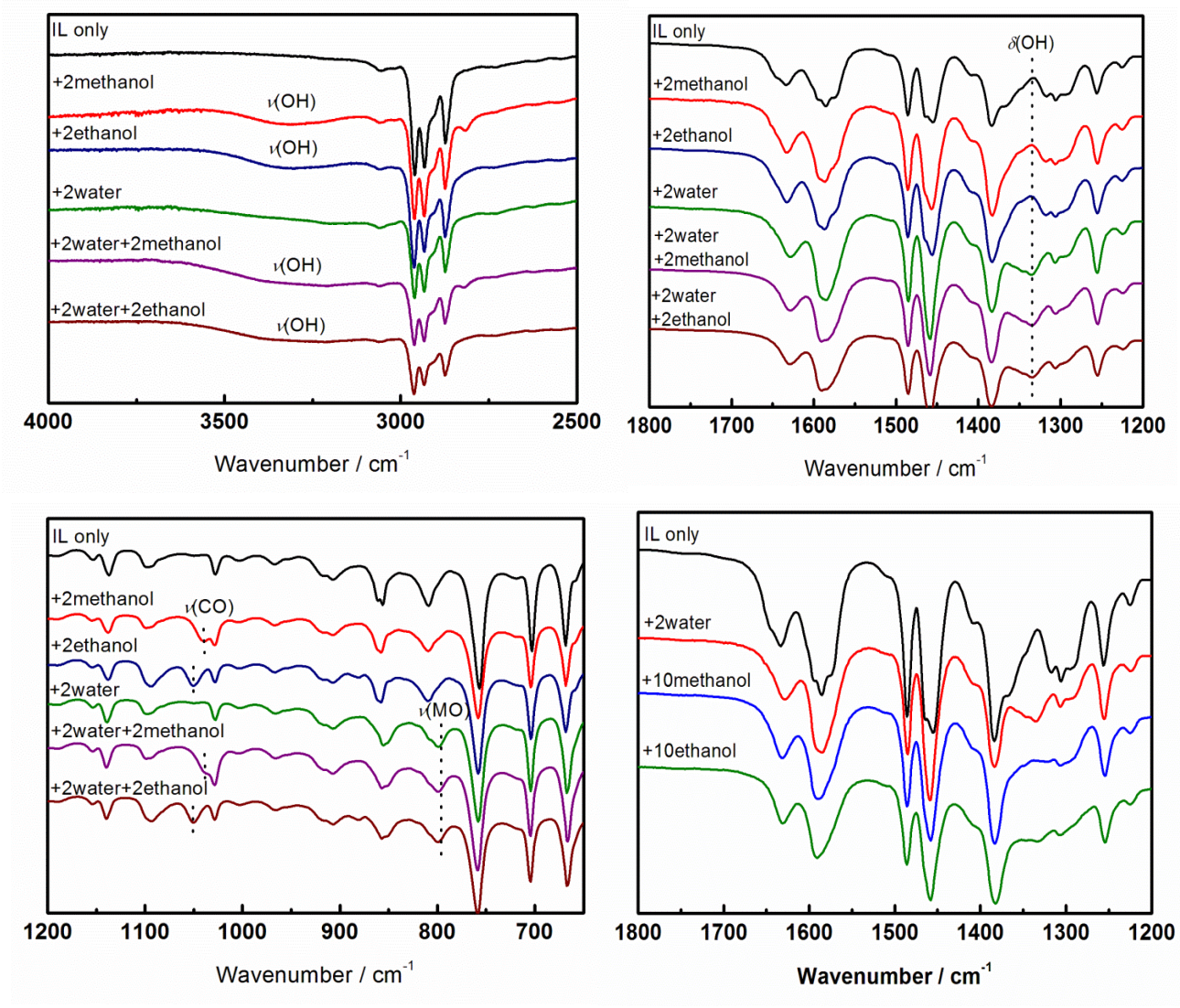

Fig. S24 ATR-FTIR spectra of $[P_{4444}]_2[Co^{II}(Sal)_2]$ after mixing with different molar equivalents of water, methanol, ethanol, and water/alcohol mixtures.

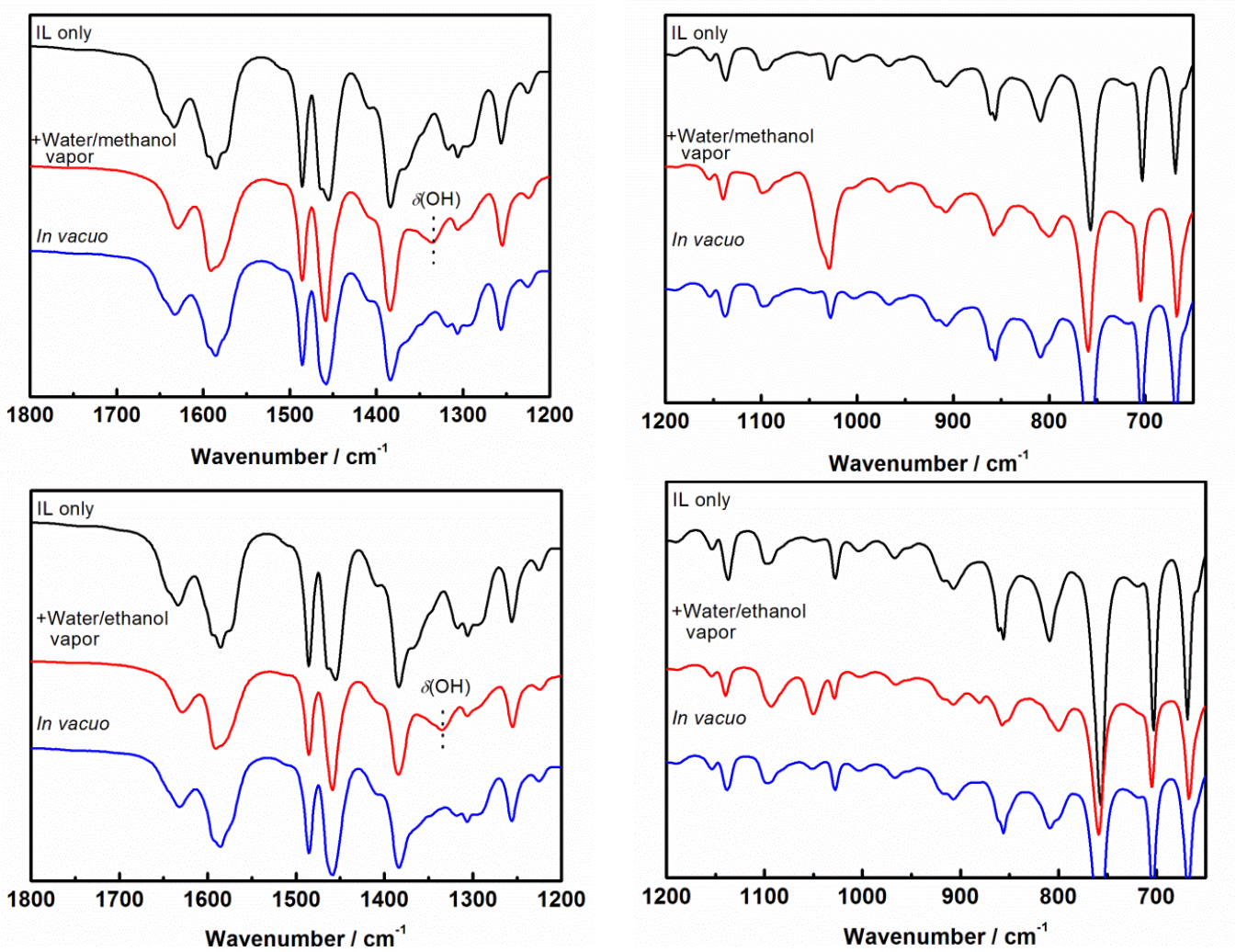

Fig. 25 ATR-FTIR spectra of $[P_{4444}]_2[Co^{II}(Sal)_2]$ before and after exposure to a mixture of (water + alcohol) vapour and then after evacuation of the water/alcohol-exposed samples.

References for the ESI

1 T. Ando, Y. Kohno, N. Nakamura and H. Ohno, *Chem. Commun.*, 2013, **49**, 10248.

2 L. Wang, S. Lu, Y. Zhou, X. Guo, Y. Lu, J. He and D. G. Evans, *Chem. Commun.*, 2011, **47**, 11002.

3 T. H. Crawford and J. Swanson, *J. Chem. Educ.*, 1971, **48**, 382.

4 E. M. Schubert, *J. Chem. Educ.*, 1992, **69**, 62.

5 D. Ostfeld and A. I. Cohen, *J. Chem. Educ.*, 1972, **49**, 829.

6 G. A. Bain and J. F. Beny, *J. Chem. Educ.*, 2008, **85**, 532.

7 J. M. Zadrozny, J. Telser and J. R. Long, *Polyhedron*, 2013, **64**, 209.

8 S. A. Cantalupo, S. R. Fiedler, M. P. Shores, A. L. Rheingold and L. H. Doerrer, *Angew. Chem. Int. Ed.*, 2012, **51**, 1000.

9 J. Faus, M. Julve, F. Lloret and M. C. Muñoz, *Inorg. Chem.*, 1993, **32**, 2013.

10 S. Hayami, K. Kato, Y. Komatsu, A. Fuyuhiro and M. Ohba, *Dalton Trans.*, 2011, **40**, 2167.

11 G. W. Everett Jr. and R. H. Holm, *Inorg. Chem.*, 1968, **7**, 776.

12 D. Kiriya, H. Chang, A. Kamata and S. Kitagawa, *Dalton Trans.*, 2006, 1377.

13 S. Aizawa, S. Iida, K. Matsuda and S. Funahashi, *Inorg. Chem*., 1996, **35**, 1338.

14 M. C. Buzzeo, A. H. Iqbal, C. M. Long, D. Millar, S. Patel, M. A. Pellow, S. A. Saddoughi, A. L. Smenton, J. F. C. Turner, J. D. Wadhawan, R. G. Compton, J. A. Golen, A. L. Rheingold and L. H. Doerrer, *Inorg. Chem.*, 2004, **43**, 7709.

15 (*a*) P. V. Khadikar, S. M. Ali and B. D. Heda, *J. Therm. Anal.*, 1985, **30**, 167; (*b*) M. C. Alvarez-Ros, S. Sánchez-Cortés and J. V. García-Ramos, *Spectrochim. Acta A*, 2000, **56**, 2471; (*c*) M. H. Soliman and G. G. Mohamed, *Spectrochim. Acta A*, 2013, **107**, 8.